Structural Asymmetry of Metallic Single-Atom Contacts Detected by Current–Voltage Characteristics

Yuji Isshiki, Dongzhe Li, Manabu Kiguchi, Tomoaki Nishino, Fabian Pauly, Shintaro Fujii

Structural Asymmetry of Metallic Single-Atom Contacts Detected by Current−Voltage Characteristics

Yuji Isshiki[1], Dongzhe Li[2], Manabu Kiguchi[1], Tomoaki Nishino[1], Fabian Pauly[3], and Shintaro Fujii[1]**

[1]Department of Chemistry, School of Science, Tokyo Institute of Technology, 2–12–1 W4-10 Ookayama, Meguro-ku, Tokyo 152–8551, Japan

[2]CEMES, Université de Toulouse, CNRS, 29 rue Jeanne Marvig, F-31055 Toulouse, France

[3]Institute of Physics, University of Augsburg, 86135 Augsburg, Germany

*e-mail: fabian.pauly@uni-a.de, fujii.s.af@m.titech.ac.jp

KEYWORDS: *electrical conductance, metallic atomic contact, break junction, current-voltage characteristics, structural asymmetry*

ABSTRACT: The complex behavior of the simplest atomic-scale conductors indicates that the electrode structure itself is significant in the design of future nanoscale devices. In this study, the structural asymmetry of metallic atomic contacts formed between two macroscopic Au electrodes at room temperature was investigated. Characteristic signatures of the structural asymmetries were detected by fast current−voltage ($I-V$) measurements with a time resolution of approximately 100 μs. Statistical analysis of more than 300,000 $I-V$ curves obtained from more than 1,000 contact-stretching processes demonstrates that the current rectification properties are correlated with the conductance of the nanocontacts. A substantial suppression of the variation in current rectification was observed for the atomic contacts with integer multiples of the conductance quantum. Statistical analysis of the time-resolved $I-V$ curves revealed that the current rectification variations increased significantly from 500 μs onwards before the breakage of the atomic contacts. Atomistic ab initio simulations of the stretching processes and corresponding $I-V$ characteristics confirmed the magnitude of the rectification and related it to the structural asymmetries in the breakdown process of the junctions. This study provides a better understanding of charge transport properties in extremely sensitive quantum point contacts, where the geometric and the electronic structure at the atomic scale are closely related each other.

INTRODUCTION

Nanocontacts fabricated using break junction and scanning probe methods have helped scientists investigate concepts in charge transport at the atomic scale [1, 2]. In the last few decades, experimental studies on charge transport across metallic atomic contacts have revealed unique quantum properties, such as electronic shell effects [3, 4], parity oscillations [5], conductance fluctuations [6], and quantum interference [6]. Most of the experiments were conducted under cryogenic conditions. At cryogenic temperatures and fixed electrode separation, an atomic contact is trapped in a specific geometrical configuration. In contrast, large variations in contact geometry can arise from thermal fluctuations at room temperature [7−11]. In this context, the linearity and nonlinearity of current versus bias voltage (I−V) characteristics of metallic atomic contacts have been investigated under thermal fluctuation conditions at room temperature [12, 13]. Hansen et al. developed a method for fast charge transport measurements to capture the transport properties of metastable states of single-atom contacts at room temperature [14]. The method detects the I−V characteristics, and has been successfully applied to reveal the linear I−V behavior of Au contacts at room temperature [14, 15]. Regarding the linearity of the I−V behavior, Tewari et al. reported shot noise measurements at liquid He temperature [16]. They revealed that the differential conductance (i.e., dI/dV) of Au atomic contacts can be both antisymmetric and asymmetric. The asymmetric character was attributed to electron backscattering from defect sites close to the atomic contact [16]. Therefore, the I−V characteristics of metallic atomic contacts are sensitive to their structural symmetry. Thus, this study aims to identify the effects of the structural symmetry of metallic atomic contacts at room temperature, which has not yet been achieved using conventional transport measurements. To this end, a fast I−V measurement setup with a high temporal resolution of approximately 100 μs was developed using the field-programmable gate array (FPGA)

technology to sample a number of metastable states of Au atomic contacts at room temperature. We demonstrate that Au atomic contacts with a conductance equal to integer multiples of the conductance quantum, $G_0 = 2e^2/h$, exhibit a suppressed asymmetry in the $I-V$ characteristics, and hence demonstrate reduced rectification effects in comparison to that of the nanocontacts with a noninteger conductance. Time course analysis of the Au atomic contacts at breakdown reveals that the structural asymmetry considerably increases starting at 500 μs before the breakage of the contacts. Thus, the Au atomic contacts were subjected to structural fluctuations, in which the contacts became asymmetric. By combining experiments and charge transport simulations, the rectifying properties of nanojunctions are related to their structural asymmetry. Consequently, this study reveals the dynamic behavior of Au atomic contacts formed during the stretching process at room temperature at a temporal resolution of approximately 100 μs.

RESULTS AND DISCUSSION

Conductance and Current Rectification Ratio of Au Atomic Contacts

Au atomic contacts were created by repeatedly forming and breaking the contact between the Au(111) substrate and Au STM tip under a bias voltage of 100 mV (Figure 1a; see also Supporting Information 1 and 2). The electrical current was recorded while forming and breaking the nanocontact. When the electrical conductance of the contact at a voltage of 100 mV ($G = I/V$) decreased to below $4G_0$ in the breaking process, the tip position was fixed, and the bias voltage was cycled between −92 and +92 mV (Figures 1b and 1c). One cycle of the voltage sweep was set to 100 μs. After the $I-V$ measurements in the self-breaking process, a nanocontact with a conductance above $4G_0$ was immediately reformed by pushing the Au STM tip toward the Au(111) substrate. Measurements in the self-breaking process mode of the atomic contacts were repeated

until a statistically significant dataset was obtained; a total of 309,600 $I-V$ curves were collected, corresponding to 2,464 self-breaking events. Figures 1d and 1e present the time evolution of the conductance and rectification behavior of an Au contact during a self-breaking process. The conductance in the positive and negative bias regimes (i.e., G_p and G_n) was calculated by linearly fitting each $I-V$ curve in the bias range from −70 to 0 mV and from 0 to +70 mV, respectively. The rectification behavior was analyzed by calculating the current rectification ratio (RR), which is defined as RR = G_p/G_n. Here, G_p and G_n are the calculated conductances at the positive and negative bias voltages, respectively. In the time evolution of the self-breaking process, the conductance features plateaus around $2.5G_0$, $2.0G_0$, $1.5G_0$, and $1.0G_0$ at both positive and negative bias voltages, which are interconnected by sudden conductance jumps (Figure 1d). Based on our measurement resolution, the conductance jumps occur within time intervals of 0.10 ms. These results indicate a diameter of only a few atoms at the narrowest cross section of the contact and spontaneous structural rearrangements during the self-breaking process [17−19]. At the end of the self-breaking process, the conductance drops from approximately $1.0G_0$ to the noise floor within 9.5 ms, which signals the breakdown of the Au single-atomic contact. Similar self-breaking behavior has been reported in the studies by Muller et al. [7] and Hansen et al. [14], in which Au contacts with conductances below $10G_0$ spontaneously broke at room temperature. While the Au atomic contacts can be held stable for rather long times on the order of an hour at low temperature, Au contacts spontaneously break at room temperature on a time scale of milliseconds owing to the diffusion of the atoms making up the contact [1]. The corresponding diffusion of Au atoms and the deformation process of Au atomic contacts at room temperature have been observed in nanoporous Au by time-resolved high-resolution transmission electron microscopy [20]. Time-resolved high-resolution transmission electron microscopy imaging on the time scale of

milliseconds (i.e., a rate of 40 frames per second) revealed that a combination of dislocation-related plastic deformations and slip-activated surface diffusion of Au atoms with a velocity of ca. 30 nm/s leads to stepwise atomistic structural changes, and finally the failure of an Au contact with an initial diameter of approximately 5 nm. The changes in conductance and RR of the Au atomic contacts, measured in the sub-millisecond time domain (Figures 1d and 1e), are attributed to structural changes in the Au contacts caused by the deformation and surface diffusion. Because the time scale of the surface diffusion of Au atoms is faster than the time resolution of this study, we expect that the measurements represent an average over different geometric configurations. By not considering the $I-V$ characteristics of Au atomic contacts with kinks, we explored Au atomic contacts before and after major structural rearrangements occurred, as discussed below thoroughly.

Figure 1e shows the time evolution of $\log_{10}$(RR), where fine variations in the current rectification behavior are apparent. In addition, the sign of $\log_{10}$(RR) is an indicator of the direction of asymmetry (positive or negative asymmetry), and the absolute value of $\log_{10}$(RR) characterizes the degree of asymmetry. Figures 2a−d present further examples of conductance plateaus with a G of approximately $1.0G_0$ and $1.5G_0$ [7, 11, 21], and their corresponding $\log_{10}$(RR). The conductance plateaus with integer multiples of the conductance quantum exhibit only small variations in G (Figure 2a) and $\log_{10}$(RR) (Figure 2b). In sharp contrast, marked fluctuations of G and $\log_{10}$(RR) are visible during the conductance plateaus with half-integer multiples of G_0 (Figures 2c and 2d). This result agrees with the observations of quantum oscillations in the thermopower, which show reduced thermopower values at integer multiples of the conductance quantum [22]. This can be explained by a particularly robust electron transmission formed by fully open transmission eigenchannels [21,23].

Statistics of Conductance and Current Rectification Ratio

We collected 309,600 $I-V$ curves to investigate the statistics of the conductance and current RR. Moreover, 31% of the 309,600 $I-V$ curves displayed kinked shapes. Such $I-V$ curves were automatically removed from the data set (Supporting Information 3) used for the statistical analysis (Figures 3 and 4), because the kinked behavior must be owing to a major dynamic structural instability of the Au contacts during a single $I-V$ measurement cycle. The kinked behavior tends to appear at higher bias conditions within the $I-V$ measurement, and after the observation of a kink, the conductance changed by approximately a conductance quantum (Supporting Information 3). Figure 3a shows a two-dimensional (2D) histogram of $\log_{10}$(RR) versus G, which was constructed using 212,279 $I-V$ curves without kinks (i.e., 69% of 309,600). It reveals three regions with high intensity counts located near $1G_0$, $2G_0$, and $3G_0$, in which $\log_{10}$(RR) is symmetrically distributed near 0. This reflects an energetic preference for Au contact geometries with a quantized conductance, and a symmetric contact structure formed on average between the Au tip and substrate. The highest-intensity regions with quantized conductance values of $2G_0$ and $3G_0$ are slightly shifted toward lower conductance values of $1.9G_0$ and $2.7G_0$, respectively. This conductance shift agrees with the results obtained in a previous study [1], in which the origin of the shift was attributed to electron backscattering on defects near the contact. In addition, we investigated the temperature dependence of the conductance and current RR statistics (Supporting Information 4). Heating to approximately 320 K suppressed the formation of geometries, exhibiting conductances of more than $1G_0$ (i.e., $2G_0$ and $3G_0$), which confirms previously reported transport measurement results at a fixed bias voltage [21, 24, 25].

To analyze the relationship between the conductance and structural symmetry of the metallic nanocontacts, $\log_{10}$(RR) histograms were constructed using a selected dataset with

conductance values in the ranges of $(1.0 \pm 0.036)G_0$, $(1.5 \pm 0.036)G_0$, and $(1.9 \pm 0.036)G_0$ (Figure 3b). The corresponding $\log_{10}$(RR) histograms were fitted using the Lorentzian function. It can be observed that the full width at half maximum (FWHM) of the Lorentzian fit w is suppressed when the conductance values are multiples of the conductance quantum. This conductance-dependent suppression of w is more clearly visible in the conductance versus w plot (Figure 3c), in which w oscillates with the conductance, and the minima of w are clearly located at multiples of G_0.

Dynamics of the Rectification Ratio before Rupture of Au Atomic Contacts

Figures 4a and 4b show an example of the last conductance plateau and corresponding $\log_{10}$(RR) before the breakage of an Au atomic contact with a conductance of $1G_0$. Immediately before the breakdown, the conductance gradually changes by approximately 30%, and finally decreases rapidly to the noise floor within 100 μs. In contrast to the conductance, $\log_{10}$(RR) shows remarkable variations with time. Initially, they are near 0; however, the magnitude of $\log_{10}$(RR) drastically increases shortly before rupture. To obtain statistical information on the dynamic behavior of the conductance and $\log_{10}$(RR), data analysis was performed as follows: First, the contact-breakdown time ($t = t_0$) was defined as the time when the conductance dropped by more than $0.5G_0$ to the noise floor in the dataset of the nonkinked 212,279 I–V curves that correspond to 1,240 self-breaking events. Because the time resolution of conductance is 0.05 ms and that of the RR is 0.1 ms, there may be no data for the RR at $t = t_0$. For example, the conductance shows $1G_0$ at $t - t_0 = 0$ and decreases to $0.3G_0$ or less at $t - t_0 = 0.05$ ms, as shown in Figure 4a, indicating that the Au atomic contact breaks at $t = t_0$. Subsequently, the RR immediately before the breakdown is defined at $t - t_0 = -0.05$, -0.15, -0.25 ms etc., as shown in Figure 4b. Among the 1,240 self-breaking events, 1,088 realizations exhibited large conductance drops with $\Delta G > 0.5G_0$.

Subsequently, $\log_{10}$(RR) histograms were generated for the dataset of 1,088 self-breaking events at $t - t_0 = -0.05, -0.15,$ and -0.25 ms (Figure 4c). The $\log_{10}$(RR) histograms illustrate a symmetric peak around 0. In Figure 4d, w of the symmetric peak is plotted as a function of time (i.e., $t–t_0$). The FWHM w starts to increase near −0.5 ms, finally growing to more than 1.5 times the value at −0.05 ms. Thus, statistical analysis of the Au atomic contact-breakdown dynamics indicates that the growing variation in $\log_{10}$(RR) signals the electrical breakdown already 0.5 ms in advance. Analysis of the evolution of $\log_{10}$(RR) suggests that 18% of the self-breaking processes (i.e., 453/2,464) exhibit a directional evolution of the asymmetry, as indicated by a monotonically increasing (decreasing) value of $\log_{10}$(RR). In 61% of the breaking processes (i.e., 1,499/2,464), $\log_{10}$(RR) instead behaves randomly and jumps between positive and negative values (Supporting Information 5).

Origin of the Rectification Behavior

Theoretical simulations based on density functional theory [26] were performed using three model structures with increasing degrees of asymmetry to explore the origin of the observed conductance and rectification behaviors of the Au atomic contacts, and to relate them to junction geometries, as shown in the top panels of Figure 5 (see also Supporting Information 6). Models 1, 2, and 3 were constructed with 4×4|3×3|3×3|4×4, 4×4|2×2|3×3|4×4, and 4×4|1×1|2×2|3×3|4×4 layers as a dynamic region, which was energetically optimized during the stretching process until the junction broke (Figure 5). Subsequently, we computed the electronic structure in the scattering region self-consistently for different bias voltages and determined the energy- and bias-dependent transmission function, $T(E,V)$, using the nonequilibrium Green's function formalism [27, 28], where the scattering region is embedded into the left and right semi-infinite electrodes via self-

energies. We employed $T(E,V)$ to obtain the charge current using the Landauer-Büttiker formula as follows [27, 28]:

$$I(V) = \frac{2e}{h}\int_{-\infty}^{+\infty} dE\, T(E,V)[f(E,\mu_{\mathrm{L}}) - f(E,\mu_{\mathrm{R}})], \qquad (1)$$

where $f(E, \mu_X)$ is the Fermi-Dirac distribution function and μ_X is the electrochemical potential of the electrode X = L, R. Finally, RR = I(+100 meV)/I(−100 meV) was evaluated by calculating the nonequilibrium charge currents at the positive and negative bias voltages of V = ±100 meV. The effect of the applied voltage V was included by shifting the electrochemical potential of the left (substrate) and right (STM tip) electrodes by $+V/2$ and $-V/2$, respectively. Let us note that because of the self-consistent electronic structure calculation, $I(V)$ is insensitive to how the bias voltage is applied, and we might also have chosen to modify, for instance, only the electrochemical potential of the substrate or, alternatively, those of the tip.

Figure 5 shows the calculated zero-bias conductance and nonequilibrium RR during the contact-stretching process. In contrast to the experiment, the stretching curves are shown as a function of pulling distance, not time. Because the mechanical properties of the flexible electrodes are expected to deviate from those of the experiment owing to the small number of dynamic atoms in the simulations, we considered the theoretically accessible electrode pulling distance.

Remarkably, variations in the conductance and $\log_{10}$(RR) of the model structures exhibit a reasonable quantitative agreement with the experimental results, as shown in Figures 1e and 2c. In particular, a relatively pronounced rectification effect is observed for model 3 at the breaking point, where the junction geometries become highly asymmetric. The agreement between the experimental and theoretical results suggests that rectification is associated with the asymmetric junction structure. In addition, the comparison between the experimental and theoretical results may be facilitated by the structural simplicity of the atomic contact at the breaking point because

only a single atom or a short chain of atoms is expected to bridge the gap between the two Au electrodes [11].

Figure 6 illustrates the energy-dependent transmission functions at ±100 mV for configurations close to the breaking point to achieve a profound insight into the rectification behavior (Supporting Information 7). Depending on the degree of junction asymmetry, the simulated transmissions deviate with respect to the polarity of the applied bias voltage, which results in the rectification property. A slight difference is found in the transmission functions for the positive and negative bias voltages of the rather symmetric models 1 and 2, while a significant difference in $T(E,\pm 100\ \text{mV})$ is observed for the asymmetric junction model 3. Therefore, the RR for model 3 is approximately one order of magnitude larger than those of models 1 and 2.

Junctions with a quantized zero-bias conductance exhibit fully transmitting eigenchannels at the Fermi energy. Thus, the transmissions of eigenchannels reach their maximum value of 1, and the full transmission $T(E, V = 0)$ consequently also exhibits a maximum as the sum of the eigenchannel transmissions. Such an extremal curve is highly robust to any changes [22, 23], including the application of a relatively small bias voltage of $|V| \leq 100$ mV. Therefore, variations in the RRs are expected to be small at zero-bias conductance values close to the quantized values nG_0, while they will grow for junctions with intermediate conductances.

CONCLUSIONS

We demonstrated that the $I-V$ characteristic of the Au atomic contacts in the low-bias regime (below 0.1 V) depends on the symmetry of the geometric structure. The $I-V$ curves of contacts at integer multiples of the conductance quantum exhibited an enhanced symmetry compared to the curves at noninteger conductance. Statistical analysis of the $I-V$ characteristics revealed that the

variation in the current rectification was suppressed in the contacts with quantized conductances. This variation demonstrated quantum oscillations as a function of conductance, which are reminiscent of thermopower and conductance fluctuations [22, 29]. Further investigations on the time-dependent $I-V$ behavior revealed that the variation of the current rectification increased significantly during the self-breaking process starting from approximately 0.5 ms before contact rupture. Therefore, the Au atomic contacts are subject to structural fluctuations before the electrical instability point, which renders the contacts asymmetric. Consequently, this study provides a profound insight into the relationship between the geometric and electronic structures of metallic atomic contacts through a fast current-voltage measurement setup under room temperature conditions.

EXPERIMENTAL METHODS

Experiment. An Au(111) surface was prepared by thermal deposition of Au on mica at elevated temperatures under high-vacuum conditions. The employed Au(111) was subsequently flame-annealed and washed with ethanol (Kanoto Chemical, purity > 99.5%) before use. A freshly cut Au wire (Nilaco, diameter ~0.3 mm, purity>99%) was used as the tip. A commercially available scanning tunneling microscopy (STM) apparatus was used with a signal access module III (Bruker, Multimode STM), in which the current amplifier and piezo driver were replaced by an SR570 (Stanford Research System) and E-663 (Physik Instrumente), respectively. The feedback loop for the STM operation was controlled using a custom-made program based on an FPGA (National Instrument, PCIe 7852R) with a sampling rate of up to 1 MHz (Supporting Information 1). Gold atomic contacts were created by repeatedly forming and breaking the contact between the Au(111) substrate and Au STM tip with a tip displacement velocity of 7.5 nm/s under a bias voltage of 100

mV (Figure 1a). The electrical current was recorded while forming and breaking the nanocontact. When the electrical conductance of the contact at 100 mV ($G = I/V$) decreased to below $4G_0$ in the breaking process, the tip position was fixed and the bias voltage was swept between −92 and +92 mV. One cycle of the voltage sweep was set to 100 μs. The voltage cycling scheme was continued $n \times 100$ times, where n is a positive integer until the atomic contact is broken. In addition, the conductance decreases to below $0.7G_0$ within the nth voltage cycling process (Figures 1b and 1c; see also Supporting Information 1). After the self-breaking process of the atomic contact at the constant tip-substrate separation, a nanocontact with a conductance above $4G_0$ was immediately reformed by pushing the Au STM tip toward the Au(111) substrate. Measurements of the self-breaking processes of the atomic contacts were repeated until a statistically significant dataset was obtained. We collected 309,600 I–V curves, which corresponded to 2,464 self-breaking events.

Calculations. Atomistic ab initio simulations of Au nanowires were carried out within the density functional theory (DFT) framework, as implemented in the plane-wave software package QUANTUM ESPRESSO [26]. The Perdew-Burke-Ernzerhof (PBE) exchange-correlation functional [30] and ultra-soft pseudopotentials [31] were used. Energy cutoffs of 30 and 300 Ry were employed for the wave functions and charge density, respectively. Supercell Au structures were obtained by extending the Au(111) unit cell in three dimensions with a 4×4 periodicity in the xy plane. The Au contacts were allowed to relax until the atomic forces fell below 10^{-3} Ry/Bohr. The Γ-point approximation was used for geometry optimization. Subsequently, based on the determined geometries, ab initio charge transport properties were computed using the software package TRANSIESTA [27, 28] and its "post-processing" code TBTRANS and SISL [32], which employs the nonequilibrium Green's function formalism combined with DFT. In these separate

DFT calculations for transport, Troullier-Martins norm-conserving pseudopotentials, the PBE exchange-correlation functional, the double-zeta polarization basis, and an energy cutoff for the real-space mesh of 250 Ry were used. A 10 × 10 × 1 **k**-point mesh was found to be sufficient to obtain well-converged transmission functions. We resolved the transmission functions on an energy mesh with a resolution of 0.02 eV.

ASSOCIATED CONTENT

Supporting Information

The Supporting Information is available free of charge at

The Supporting Information discusses the temporal resolution of the current measurement setup, examples of *I*−*V* measurements with time evolution, analysis of the *I*−*V* curves of Au atomic contacts, temperature dependence of conductance and RR, evolution of junction asymmetry, distribution of elongation lengths until rupture, and DFT simulations of Au atomic contacts.

ACKNOWLEDGMENTS

This work was financially supported by Grants-in-Aid for Scientific Research (No. 20K05245), JST CREST (No. JP-MJCR18I4), JSPS Fellows (19J21186) from MEXT Japan, and the Precise Measurement Technology Promotion Foundation (PMTPF). This work was performed using HPC resources from CALMIP (Grant 2021-P21008).

AUTHOR INFORMATION

Author Contributions

All authors contributed in writing the manuscript. All authors approved the final version of the manuscript.

Notes

The authors declare no competing financial interest.

REFERENCES

[1] Agraït, N.; Yeyati, A. L.; van Ruitenbeek, J. M. Quantum Properties of Atomic-Sized Conductors, *Phys. Rep.* **2003**, 377, 81–279.

[2] van Ruitenbeek J. M. Conductance Quantization in Metallic Point Contacts. Metal Clusters at Surfaces. Springer Series in Cluster Physics. Springer, Berlin, Heidelberg **2000**.

[3] Yanson, A. I.; Yanson, I. K.; van Ruitenbeek, J. M. Observation of Shell Structure in Sodium Nanowires, *Nature* **1999**, 400, 144–146.

[4] Mares, A. I.; Otte, A. F.; Soukiassian, L. G.; Smit, R. H. M.; van Ruitenbeek, J. M. Observation of Electronic and Atomic Shell Effects in Gold Nanowires, *Phys. Rev. B* **2004**, 70, 073401.

[5] Smit, R. H. M.; Untiedt, C.; Rubio-Bollinger, G.; Segers, R. C.; van Ruitenbeek, J. M. Observation of a Parity Oscillation in the Conductance of Atomic Wires, *Phys. Rev. Lett.* **2003**, 91, 076805.

[6] Ludoph, B.; Devoret, M. H.; Esteve, D.; Urbina, C.; van Ruitenbeek, J. M. Evidence for Saturation of Channel Transmission from Conductance Fluctuations in Atomic-Size Point Contacts, *Phys. Rev. Lett.* **1999**, 82, 1530–1533.

[7] Muller, C. J.; Krans, J. M.; Todorov, T. N.; Reed, M. A. Quantization Effects in the Conductance of Metallic Contacts at Room Temperature, *Phys. Rev. B* **1996**, 53, 1022–1025.

[8] Rubio, G.; Agraït, N.; Vieira, S. Atomic-Sized Metallic Contacts: Mechanical Properties and Electronic Transport, *Phys. Rev. Lett.* **1996**, 76, 2302–2305.

[9] Kizuka, T. Atomic Process of Point Contact in Gold Studied by Time-Resolved High-Resolution Transmission Electron Microscopy, *Phys. Rev. Lett.* **1998**, 81, 4448–4451.

[10] Kizuka, T. Atomic Configuration and Mechanical and Electrical Properties of Stable Gold Wires of Single-Atom Width, *Phys. Rev. B* **2008**, 77, 155401.

[11] Dreher, M.; Pauly, F.; Heurich, J.; Cuevas, J. C.; Scheer, E.; Nielaba, P. Structure and Conductance Histogram of Atomic-Sized Au Contacts, *Phys. Rev. B* **2005**, 72, 075435.

[12] Yoshida, M.; Oshima, Y.; Takayanagi, K. Nonlinear Current−Voltage Curves of Gold Quantum Point Contacts. *Appl. Phys. Lett*. **2005**, 87, 103104.

[13] Costa-Krämer, J. L.; García, N.; García-Mochales, P.; Serena, P. A.; Marqués, M. I.; Correia, A. Conductance Quantization in Nanowires Formed between Micro and Macroscopic Metallic Electrodes. *Phys. Rev. B*, **1997**, 55, 5416−5424.

[14] Hansen, K.; Nielsen, S. K.; Legsgaard, E.; Stensgaard, I.; Besenbacher, F. Fast and Accurate Current−Voltage Curves of Metallic Quantum Point Contacts, *Rev. Sci. Instrum.* **2000**, 71, 1793–1803.

[15] Hansen, K., Nielsen, S. K., Brandbyge, M., Lægsgaard, E., Stensgaard, I., Besenbacher, F. Current−Voltage Curves of Gold Quantum Point Contacts Revisited, *Appl. Phys. Lett*. **2000**, 77, 708–710.

[16] Tewari, S.; van Ruitenbeek, J. M.; Anomalous Nonlinear Shot Noise at High Voltage Bias, *Nano Lett.* **2018**, 18, 5217−5223.

[17] Yanson, A. I.; Bollinger, G. R.; van den Brom, H. E.; Agraït, N.; van Ruitenbeek, J. M. Formation and Manipulation of a Metallic Wire of Single Gold Atoms. *Nature* **1998**, 395, 783–785.

[18] Tsutsui, M.; Shoji, K.; Taniguchi, M.; Kawai, T. Formation and Self-Breaking Mechanism of Stable Atom-Sized Junctions, *Nano Lett.* **2008**, 8, 345–349.

[19] Tsutsui, M.; Chen, Y.-C. Heat Dissipation in Quasi-Ballistic Single-Atom Contacts at Room Temperature, *Sci. Rep.* **2019**, 9, 18677.

[20] Liu, P.; Wei, X.; Song, S.; Wang, L.; Hirata, A.; Fujita, T.; Han, X.; Zhang, Z.; Chen, M. Time-Resolved Atomic-Scale Observations of Deformation and Fracture of Nanoporous Gold under Tension, *Acta Mater*. **2019**, 165, 99−108.

[21] Mosso, N.; Drechsler, U.; Menges, F.; Nirmalraj, P.; Karg, S.; Riel, H.; Gotsmann, B. Heat Transport through Atomic Contacts, *Nat. Nanotech*. **2017**, 12, 430–433.

[22] Evangeli, C.; Matt, M.; Rincon-Garcia, L.; Pauly, F.; Nielaba, P.; Rubio-Bollinger, G.; Cuevas, J. C.; Agraït, N. Quantum Thermopower of Metallic Atomic-Size Contacts at Room Temperature. *Nano Lett.* **2015**, 15, 1006–1011.

[23] Pauly, F.; Viljas, J. K.; Bürkle, M.; Dreher, M.; Nielaba, P.; Cuevas, J. C., Molecular Dynamics Study of the Thermopower of Ag, Au, and Pt Nanocontacts. *Phys. Rev. B* **2015**, 84, 195420.

[24] Cui, L.; Jeong, W.; Hur, S.; Matt, M.; Klöckner, J. C.; Pauly, F.; Nielaba, P.; Cuevas, J. C.; Meyhofer, E.; Reddy, P. Quantized Thermal Transport in Single-Atom Junctions, *Science* **2017**, 355, 1192−1195.

[25] Mosso, N.; Prasmusinto, A.; Gemma, A.; Drechsler, U.; Novotny, L.; Gotsmann, B. Quantized thermal conductance in metallic heterojunctions, *Appl. Phys. Lett.* **2019,** 114, 123102.

[26] Giannozzi, P.; Baroni, S.; Bonini, N.; Calandra, M.; Car, R.; Cavazzoni, C.; Ceresoli, D.; Chiarotti, G. L.; Cococcioni, M.; Dabo, I.; Dal Corso, A.; de Gironcoli, S.; Fabris, S.; Fratesi, G.; Gebauer, R.; Gerstmann, U.; Gougoussis, C.; Kokalj, A.; Lazzeri, M.; Martin-Samos, L.; Marzari, N.; Mauri, F.; Mazzarello, R.; Paolini, S.; Pasquarello, A.; Paulatto, L.; Sbraccia, C.; Scandolo, S.; Sclauzero, G.; Seitsonen, A. P.; Smogunov, A.; Umari, P.; Wentzcovitch, R. M. QUANTUM ESPRESSO: a Modular and Open-Source Software Project for Quantum Simulations of Materials, *J. Phys.: Condens. Matter* **2009,** 21, 395502.

[27] Brandbyge, M.; Mozos, J.-L.; Ordejón, P.; Taylor, J.; Stokbro, K. Density-Functional Method for Nonequilibrium Electron Transport, *Phys. Rev. B* **2002**, 65, 165401.

[28] Papior, N.; Lorente, N.; Frederiksen, T.; García, A.; Brandbyge, M. Improvements on Non-Equilibrium and Transport Green Function Techniques: The Next-Generation Transiesta, *Comput. Phys. Commun.* **2017**, 212, 8−24.

[29] Ludoph B.; van Ruitenbeek J. M. Conductance Fluctuations as a Tool for Investigating the Quantum Modes in Atomic-Size Metallic Contacts. *Phys. Rev. B* **2000**, 61, 2273.

[30] Perdew, J. P.; Burke, K.; Ernzerhof, M. Generalized Gradient Approximation Made Simple. *Phys. Rev. Lett.* **1996**, 77, 3865.

[31] Vanderbilt, D. Soft Self-Consistent Pseudopotentials in a Generalized Eigenvalue Formalism, *Phys. Rev. B* **1990**, 41, 7892.

[32] Papior, N. *sisl*: v0.9.6. (2019), https://doi.org/10.5281/zenodo.597181.

Figures

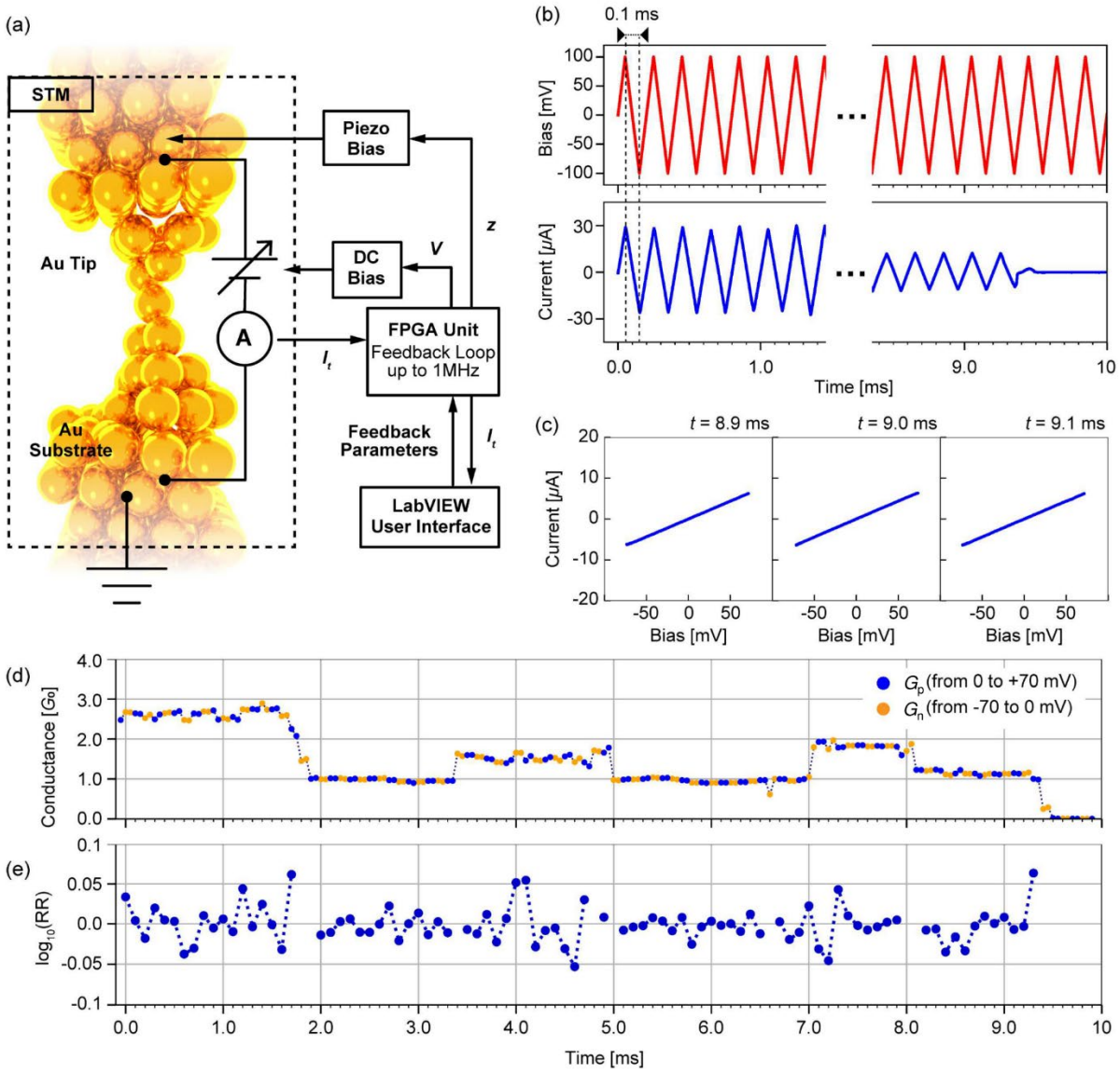

Figure 1. (a) Schematic of the experimental setup. (b) Applied bias voltage (V) and example of measured current (I) though an Au atomic contact. (c) Example of I–V characteristics at 8.9, 9.0, and 9.1 ms in (b). (d) Example of conductance at positive (blue dots) and negative (orange dots) bias voltages. (e) Logarithmically scaled current rectification ratio (RR) as a function of time, defined as RR = G_p/G_n. Here, G_p and G_n are the conductances at the positive and negative bias voltages, respectively, which are defined by the slope of each I–V curve. Data points that

correspond to the kinked $I-V$ curves are not plotted in (e), because they arise from pronounced dynamic structural changes of the Au contact occurring within the duration of an $I-V$ measurement. Details are provided in the Supporting Information.

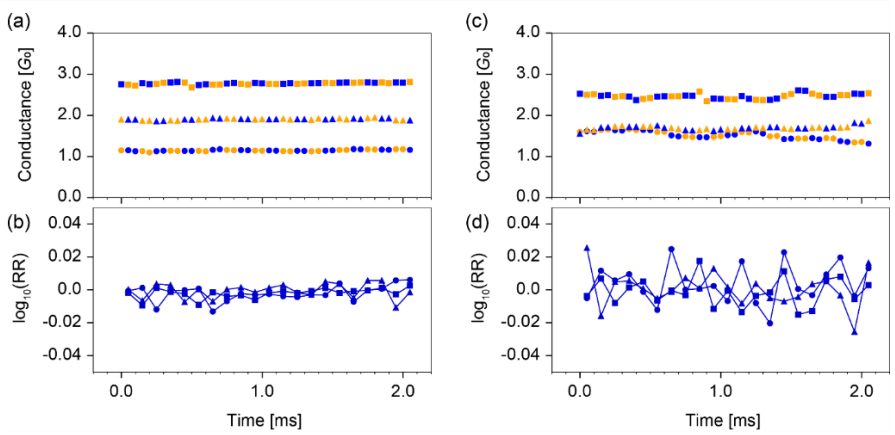

Figure 2. Examples of the time evolution of (a,c) conductance and (b,d) rectification ratio (RR). Conductance plateaus (a) near quantized values of $1.1G_0$, $1.9G_0$, and $2.8G_0$, and (c) near noninteger conductances of $1.5G_0$, $1.7G_0$, and $2.5G_0$.

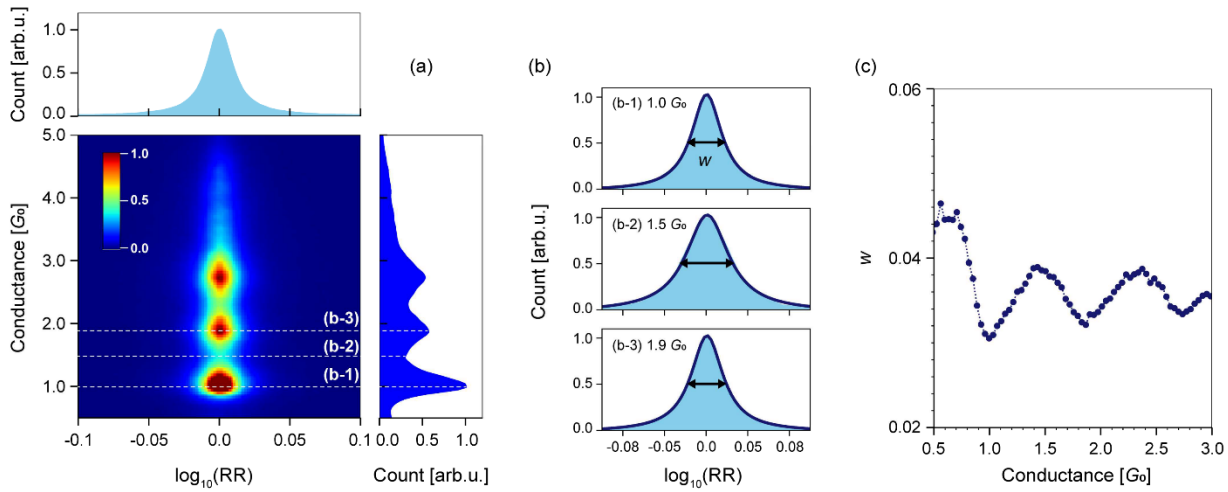

Figure 3. (a) Contour plot of counts for corresponding conductance and logarithmically scaled RR values as extracted from 212,279 nonkinked $I-V$ curves. The histogram was smoothed using the adjacent data. One-dimensional histograms of the conductance and RR are shown in the top and right panels. (b) Histograms of RR at conductances of (b-1) $1.0G_0$, (b-2) $1.5G_0$, and (b-3) $1.9G_0$, which correspond to the conductances at the white dashed lines in panel (a). All histograms were fitted using the Lorentzian functions, and the width w was defined as FWHM. (c) w vs. conductance.

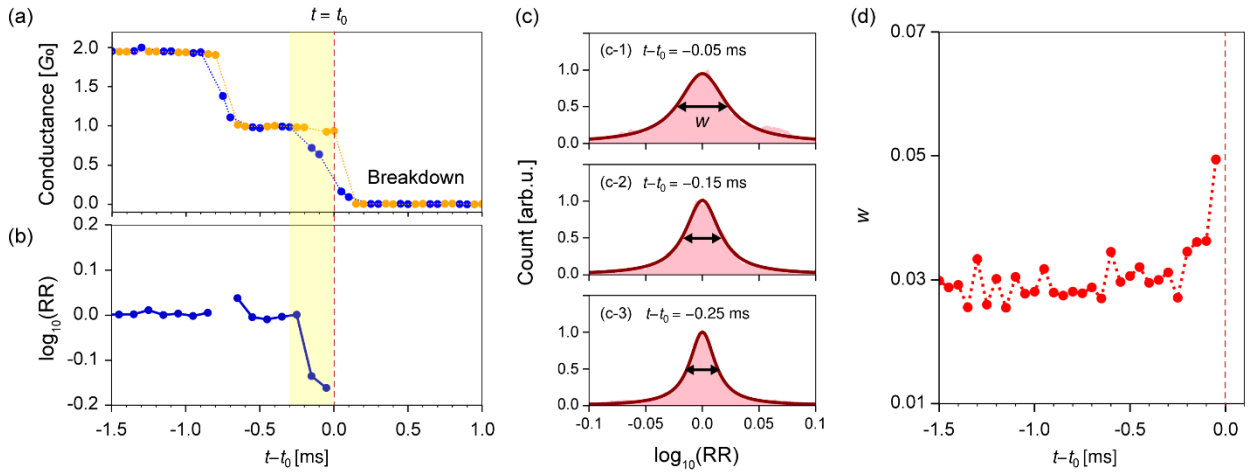

Figure 4. Example of the time evolution of (a) conductance and (b) RR before breakage of an Au atomic contact. Here, t_0 is defined as the time when the conductance decreases by more than $0.5G_0$ to the noise floor, which is located below $0.5G_0$. The blue and orange circles in (a) correspond to conductance data at positive and negative bias voltages, respectively. (c) RR histograms at the times $t-t_0 = -0.05$, -0.15, and -0.25 ms. All histograms were constructed using the data from 1,088 self-breaking events. The histograms are fitted using the Lorentzian functions, where w is defined as the FWHM. (d) w as a function of time before rupture of the Au atomic contacts.

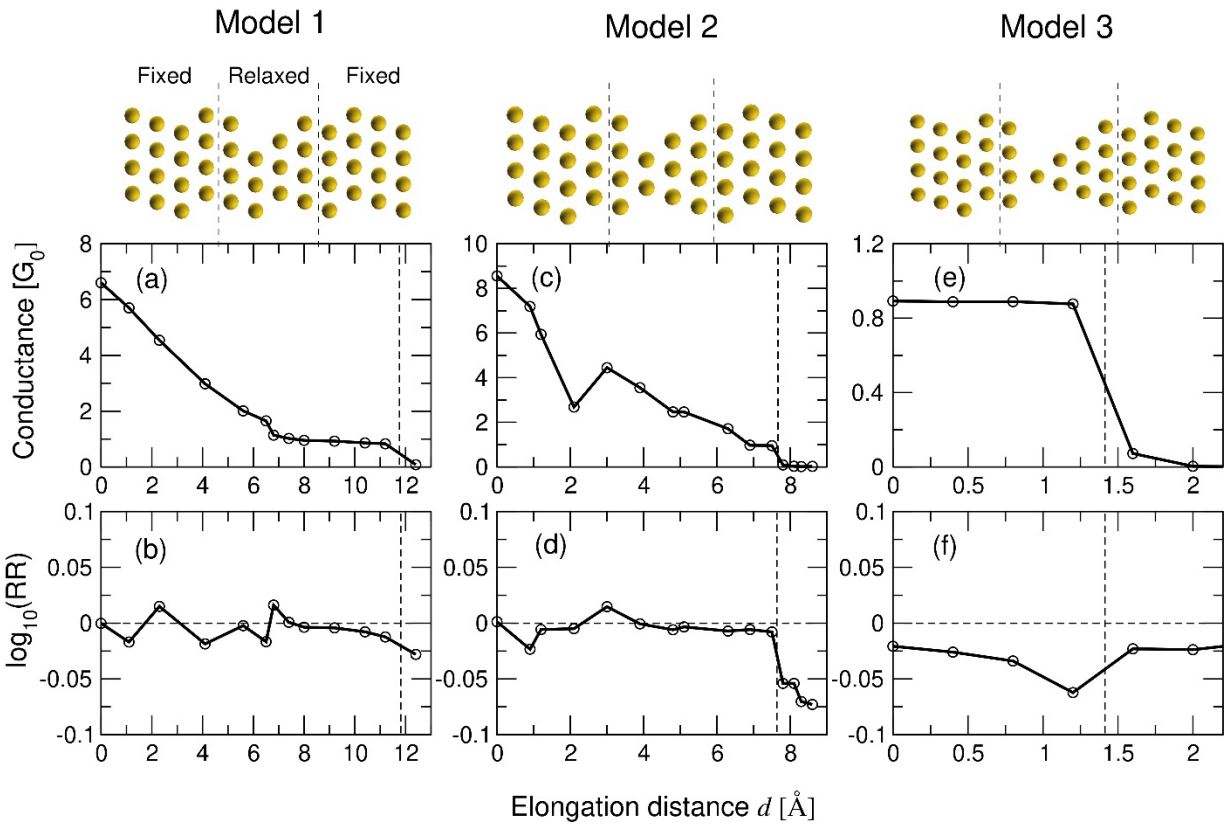

Figure 5. Evolution of the zero-bias conductance and nonequilibrium RR on a logarithmic scale during the stretching process for (a,b) model 1, (c,d) model 2, and (e,f) model 3. The vertical dashed lines represent the breaking point of the junction, defined as the elongation distance at which the conductance falls to values below $0.1G_0$. The starting configurations of the pulling process are shown above the panels. The vertical dashed lines in the configuration plots separate fixed electrode regions on the left and right from the dynamical region in the center, where atomic positions are determined by the search of an energy minimum throughout the pulling process. The RR increases noticeably near the breaking point for the asymmetric

junction model 3, whereas the effect is less pronounced for models 1 and 2 with rather symmetric initial configurations.

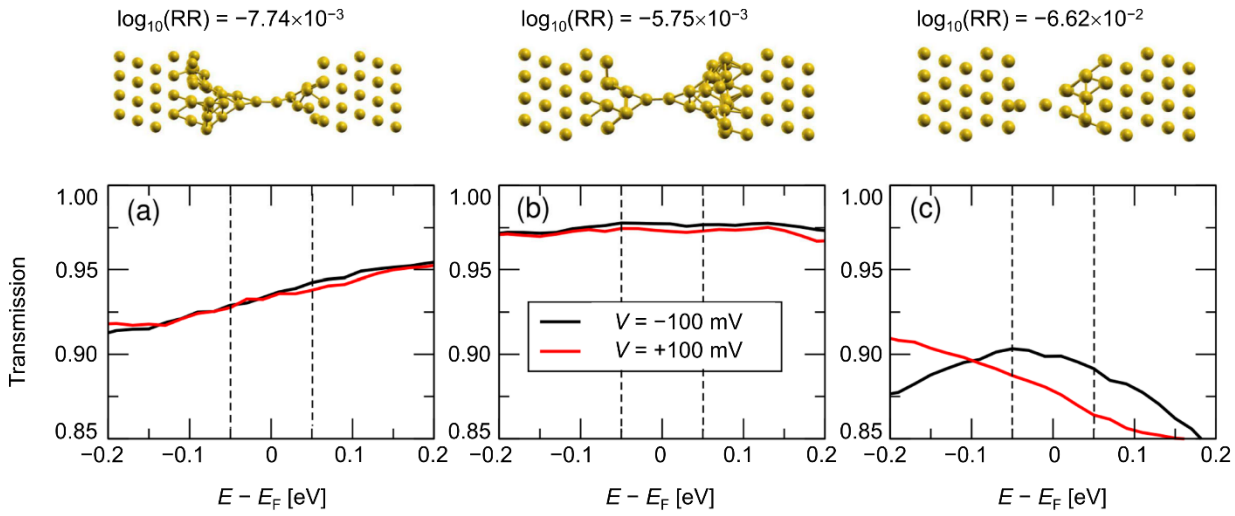

Figure 6. Energy-dependent transmission functions at -100 (black) and +100 meV (red) for (a) model 1 at an electrode separation d = 10.4 Å, (b) model 2 at d = 6.9 Å and (c) model 3 at d = 1.2 Å. The dashed vertical lines represent the integration energy window used for the transport calculations. It is consistently chosen with the symmetric application of the bias voltage to the left and right electrodes in the self-consistent electronic structure calculations.

TOC

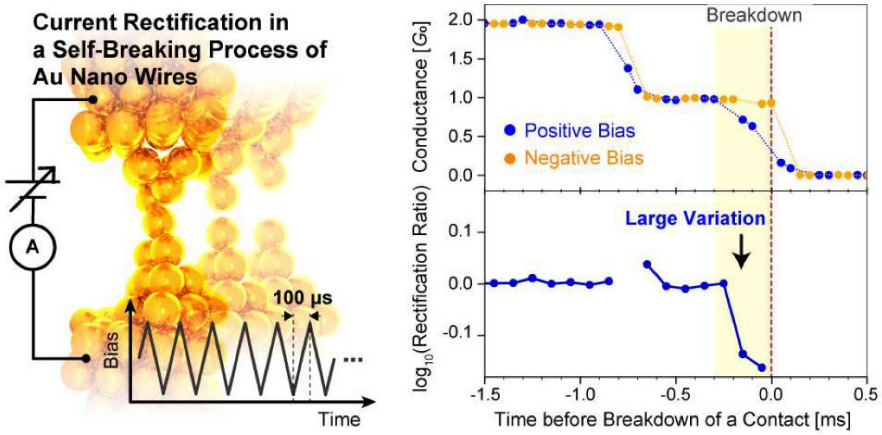
Current Rectification in
a Self-Breaking Process of
Au Nano Wires
A
100 μs
Bias
Time
Breakdown
Positive Bias
Negative Bias
Large Variation
Conductance [G0]
log10(Rectification Ratio)
Time before Breakdown of a Contact [ms]